Current Applied Physics 14 (2014) 856–861

Contents lists available at ScienceDirect

Current Applied Physics

journal homepage: www.elsevier.com/locate/cap

Thickness effect of the TiO_2 nanofiber scattering layer on the performance of the TiO_2 nanoparticle/TiO_2 nanofiber-structured dye-sensitized solar cells

Ji-Hye Lee [a], Kyun Ahn [a], Soo Hyung Kim [a], Jong Man Kim [a], Se-Young Jeong [b], Jong-Sung Jin [c], Euh Duck Jeong [c], Chae-Ryong Cho [a,*]

[a] Department of Nano Fusion Technology, Pusan National University, Miryang 627-706, Republic of Korea
[b] Department of Cogno-Mechatronics Engineering, Pusan National University, Busan 609-735, Republic of Korea
[c] Division of High Technology Materials Research, Korea Basic Science Institute, Busan 618-230, Republic of Korea

ARTICLE INFO

Article history:
Received 4 February 2014
Accepted 1 April 2014
Available online 13 April 2014

Keywords:
TiO_2 nanofiber
Scattering layer
Dye-sensitized solar cells
Double-layered photoanode

ABSTRACT

TiO_2 nanofibers (NFs) were fabricated by an electrospinning process and were used as scattering layers in dye-sensitized solar cells (DSSCs). The NF-coated photoanodes of the DSSCs were prepared with a variety of scattering layer thicknesses. The thickness effect of the scattering layer on the double-layered TiO_2 nanoparticle (NP)/TiO_2 NF structure was investigated through structural, morphological, and optical measurements. In the double-layered photoanode, the TiO_2 NP layer plays a major role in dye adsorption and light transmission, and the TiO_2 NF scattering layer improves the absorption of visible light due to the light scattering effects. The scattering effect of TiO_2 NFs layer was examined by the incident monochromatic photon-to-electron conversion efficiency (IPCE) and UV–Vis spectrometry. The conversion efficiency for the 12 μm-thick photoanode composed of a 2 μm-thick TiO_2 NF layer and 10 μm-thick TiO_2 NP layer was higher than that of DSSCs with only TiO_2 NPs photoanode by approximately 33%.

1. Introduction

Dye-sensitized solar cells (DSSCs) have continued to excite interest in academic research and industrial applications since Gratzel et al. first reported such a device in 1991 [1]. DSSCs have a variety of advantages compared to conventional devices, such as low-cost material components, high stability, cost-effective solar energy conversion, and simple fabrication schemes on both rigid and flexible substrates. Typical DSSCs consist of a TiO_2 nanoparticle (NP) film covered by chemisorbed dye molecules as a photoanode, redox electrolyte, and counter electrode, arranged in a stack.

The TiO_2 NP film, which adsorbs dyes, separates and transfers charges, and scatters light, is perhaps the most important component in a DSSC [2]. In particular, TiO_2 NPs with sizes 10–30 nm have mainly been used as photoanode materials in DSSCs because their large surface areas adsorb more dye molecules, and, in turn, provide more effective photocurrent generation [3]. However, a photoanode of dye-coated TiO_2 NPs shows low light absorption of the dye, inefficiencies related to visible light scattering effects, and charge trapping at grain boundaries, resulting in a significant loss of the incident light and reduction in the power generated [4]. Among these, the improvement of light scattering at the photoanode becomes important to enhance the efficiency of DSSCs. Many efforts have been devoted to develop highly efficient TiO_2 photoanodes; some important strategies incorporate one-dimensional materials such as nanowires (NWs), nanotubes (NTs), nanorods (NRs), and nanofibers (NFs) [5–7]. Such 1D nanostructures have many advantages such as good light scattering and electron transport properties compared to the bulk materials.

One approach to improving the light harvesting capabilities of the photoanode without sacrificing surface area is the formation of an upper scattering layer on the TiO_2 NP photoanode. It has been reported that a TiO_2 NP photoanode with such an upper layer exhibits increased radiation path lengths within the film, which improves the harvesting of photons while maintaining dye loading levels [8]. Many researchers have demonstrated that the optical absorption of TiO_2 NP films can be improved by the addition of large TiO_2 particles as a scattering layer [4,9–11]. The introduction

* Corresponding author. Department of Nano Fusion Technology (Jayul, room 639), College of Nanoscience and Nanotechnology, Pusan National University, 50 chonghak-ri, Samnangjin-eup, Miryang 627-706, Republic of Korea. Tel.: +82 55 350 5297; fax: +82 55 353 1314.
E-mail addresses: crcho@pusan.ac.kr, crcho9113@naver.com (C.-R. Cho).

http://dx.doi.org/10.1016/j.cap.2014.04.001
1567-1739/

of 1D nanostructures as an upper scattering layer on TiO_2 NPs film is an active field of research. (See, for example: NP/NR systems [12], NP/NT systems [13], and NP/NF systems [14–17].) In particular, in the TiO_2 NP/NF double-layered photoanode structure, it is believed that the NP layer plays a major role in dye adsorption and light transmission and that the NF layer improves absorption in the visible light range by the light scattering effect. However, there is currently no report describing the influence of the relative thicknesses of the NF and NP layers on cell performance.

In this study, we report that the formation of a crystalline TiO_2 NF light scattering layer on a TiO_2 NP layer enhances light absorption by dyes in DSSCs. Because surface area and scattering effects are counterbalanced, controlling the thicknesses of both the scattering layer and the lower NP layer in the double-layered structure is important in the fabrication of the double-layered structure. We investigated the cell efficiency according to the thickness of the TiO_2 NF layer through the structural, morphological, and optical measurements of the double-layered photoanodes. Our double-layered structure is composed of an upper TiO_2 NF layer (as a scattering layer) and a lower TiO_2 NP layer (the so-called P25 layer) (Fig. 1).

2. Experimental details

2.1. Preparation of TiO_2 NPs and TiO_2 NFs

TiO_2 NPs (P25, ~21 nm particle size) were purchased from Sigma–Aldrich and the TiO_2 NFs were fabricated by an electrospinning method. To fabricate the electrospinning precursor solution, 0.9 g polyvinyl pyrrolidone (PVP) was mixed with 7 mL ethanol and stirred at room temperature for 1 h. After adding 1.485 g titanium isopropoxide in 3.5 mL ethanol and 1 mL acetic acid, the solution was stirred for 3 h. All materials were obtained from Sigma–Aldrich and used without further purification. Electrospinning was carried out at a flow rate of 0.5 mL/h and a voltage of 15 kV. The electrospun TiO_2 NFs were annealed at 500 °C for 2 h to remove the volatile organic compounds and crystallize the specimen.

2.2. Synthesis of TiO_2 NP and TiO_2 NF pastes

Pastes were prepared by first mixing 0.30 g of the TiO_2 NP and TiO_2 NF with 0.05 mL acetic acid, respectively and then dispersing them in this solution by ultrasonication for 10 min. During ultrasonication, distilled water and ethanol were repeatedly added and then stirred and ultrasonicated several times. After adding 1.07 mL terpinol to this solution, the mixed solution was stirred and ultrasonicated one more time. Next, 0.15 g ethyl cellulose was mixed with 1.90 mL ethanol and stirred at elevated temperature in order to melt it. The solution containing ethyl cellulose was combined with TiO_2 nanostructure solution and ultrasonicated. After evaporation of ethanol at 80 °C, the TiO_2 NP and TiO_2 NF pastes were finally obtained, respectively.

2.3. Fabrication of DSSCs

All photoanodes were fabricated on the FTO/glass substrates. The FTO/glass was then treated with an aqueous solution of $TiCl_4$ (2 mM) at 95 °C for 30 min. Following the $TiCl_4$ treatment, the substrates were washed with ethanol and then dried and sintered at 500 °C. By the screen printing method, the FTO/glass substrates were first coated with the TiO_2 NP paste, and then with the NF paste, over 5 mm × 5 mm sized regions. After coating the NP/NF pastes, the substrates were finally annealed at 500 °C for 2 h.

The morphology/thickness of the TiO_2 nanostructured films affects dye loading; higher dye loading is one of the factors that leads to higher efficiency. The optimum TiO_2 thickness is believed to be 12–14 μm [2]. Herein, we fabricated three types of TiO_2 nanostructures. The total thickness of the TiO_2 NP/NF double layer was 12 μm, and the thickness of the NF scattering layer, considering

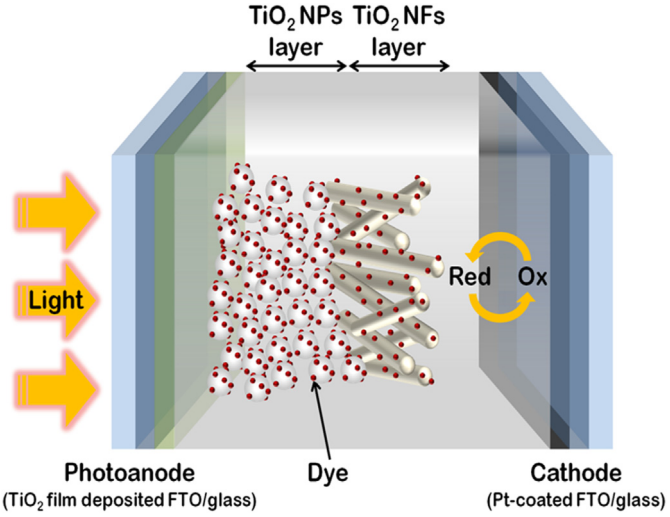

Fig. 1. Schematic diagram of double-layered DSSCs composed of TiO_2 NF layer on top of NP layer.

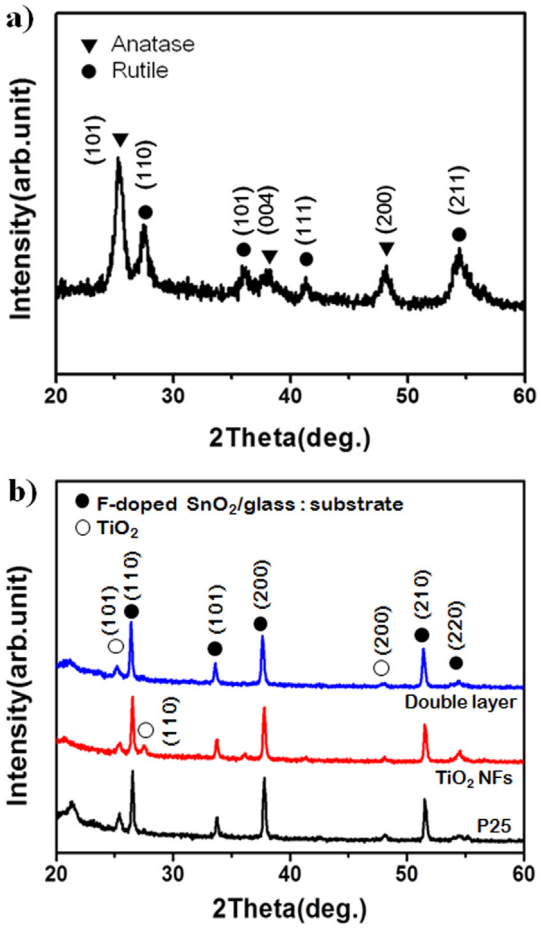

Fig. 2. XRD patterns of (a) TiO_2 NFs and (b) TiO_2 photoanodes coated on FTO/glass substrate. "Double-layer" denotes TiO_2 NFs coated on P25 layer.

thickness (~2 μm) per number of screen-printing, was 2, 4, and 6 μm, respectively. The $TiCl_4$ treatment for TiO_2 NFs layer was carried out for increasing the adsorption of dye molecules. A photoanode with the NP layer was prepared but without the NFs layer for use as a reference device for measuring the scattering effect. All photoanodes were immersed in a solution of N719 dye (Solaronix) for 24 h. Then, the dye-sensitized photoanodes were washed with ethanol to remove unanchored dye molecules. Platinum-coated FTO/glass was used as the counter electrode. The dye-adsorbed TiO_2 photoanode and counter electrode were assembled into a sandwich-type device in which the internal space between the electrodes was filled with a liquid electrolyte (Iodolyte AG-50, Solaronix).

2.4. Device characterization

The crystal structures of the TiO_2 NFs and the double-layered photoanodes were determined using an X-ray diffractometer (XRD) [Phillips, X'pert Pro] in the $\theta-2\theta$ scan mode with 2θ ranging from 20° to 60° and Cu-$K_{\alpha 1}$ radiation (wavelength $\lambda = 1.5406$ Å). The morphological properties of these samples were investigated with a field-emission scanning electron microscope (FE-SEM) [Hitachi, S-4700] at an operating voltage of 15 kV. The absorbance and transmittance of the photoanodes were measured using an ultraviolet–visible spectrometer [Scinco, S-3100] over the region 400–800 nm. The incident photon-to-electron conversion efficiency (IPCE) was characterized using a solar simulator [Abet Technologies Inc., Sun 2000] with an arc lamp light source [Abet Technologies Inc., LS-150-Xe] that provides illumination over the wavelength range 400–800 nm. The electrochemical impedance spectroscopy (EIS) measurements were made over the frequency range 0.1–100 kHz using an open-circuit voltage with a potential pulse of amplitude 10 mV. The current density–voltage ($J-V$) characteristics of the DSSCs were measured under AM 1.5 simulated illumination with an intensity of 100 mW/cm^2 [Peccell Technologies Inc., PEC-L12]. The intensity of illumination in terms of sunlight was calibrated using a standard Si photodiode detector with a KG-5 filter.

3. Results and discussion

Fig. 2 shows the XRD patterns of the TiO_2 NFs and photoanode films on the FTO/glass substrates. The specimens were pure, crystalline TiO_2; no peaks for other impurity phases were observed. All observed diffraction peaks for the TiO_2 NFs agreed with those reported for TiO_2, as shown in Fig. 2(a). The peaks at 25.3° and 27.4° indicate that both the anatase (101) and rutile (110) phases are present. Fig. 2(b) shows the XRD patterns of photoanodes with three different TiO_2 structures on the FTO/glass. The TiO_2 peaks are less intense than those of FTO because the nanosized and randomly oriented TiO_2 NPs and NFs provide comparatively reduced signal than the FTO. The TiO_2-indexed peaks correspond to the (101), (110), and (200) reflections at 25.4°, 27.5°, and 48.1°, respectively. The photoanode peaks also agree with the crystalline TiO_2 phases, even though anatase and rutile peaks cannot be clearly resolved because of the weak overall peak intensities. These three samples exhibited similar intensities because that they have the same total nanostructured layer thickness. No secondary phases were observed in any of these samples.

The cross-sectional and surface FE-SEM images of the photoanodes are shown in Fig. 3. Both the single-layered P25 and double-layered NP/NF photoanodes consist of approximately 12-μm-thick TiO_2 nanostructures. As shown in Fig. 3(a) and (b), a dense, uniform P25 photoanode was fabricated by the screen printing method. Fig. 3(c) is the FE-SEM cross-sectional image of TiO_2 NFs (4 μm thickness) coated on P25 (8 μm thickness) in the double-layered photoanode. Fig. 3(d) shows the enlarged surface morphology of TiO_2 NFs that acts as light scattering core. The average diameter of the NFs was approximately 450 nm. The TiO_2 NFs were uniform in shape and organized into smooth surfaces. The cross-section of the TiO_2 NFs shows that the TiO_2 NF layer persists during the coating and annealing processes. However, we observed some particulates

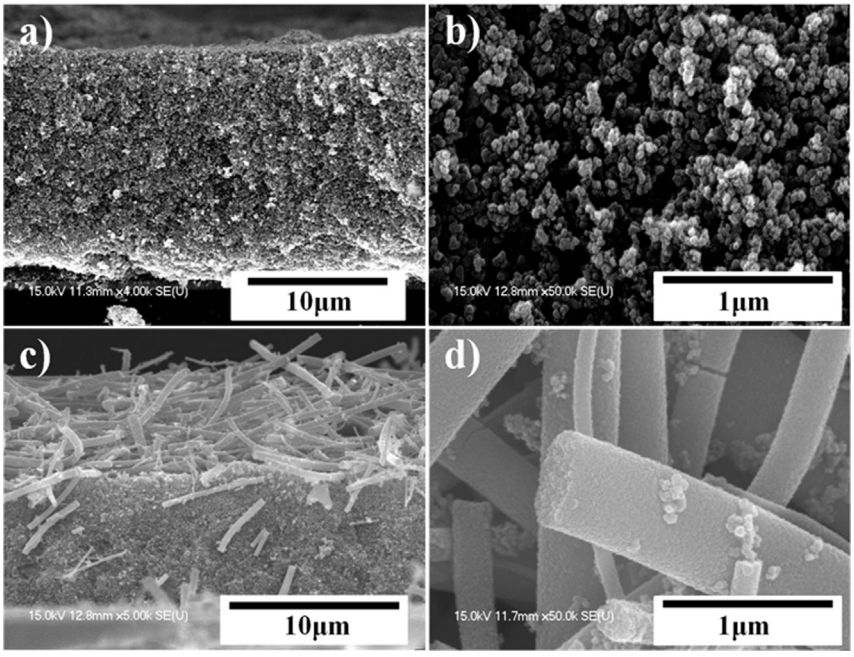

Fig. 3. SEM (a, c) cross-section and (b, d) surface images of TiO_2 NP layers only and double-layered photoanode composed of 4-μm-thick TiO_2 NF layer and 8-μm-thick TiO_2 NP layer. To clearly distinguish interface between NP and NF layers, cross-section of double-layered photoanode with 4-μm-thick TiO_2 NFs is displayed.

adhered to the NFs. We considered that these may be introduced by unintentional mixing at the interface region during the annealing of P25 and NFs or particles separated from the P25 layer during breaking the sample for SEM. Though the NFs coated on NPs appear loose, they are in fact tightly adhered to each other, and no delamination due to poor interfacial adhesion was observed.

To quantify the light scattering capabilities of the TiO_2 nanostructures, the transmittance and absorbance of the TiO_2 NPs, TiO_2 NFs, and double-layered photoanodes were measured (Fig. 4). TiO_2 NPs transmit light, but TiO_2 NFs, as 1D nanostructures, may scatter light in the visible region. As shown in Fig. 4(a), (c) and (e), the transmittance gradually decreases with increasing film thickness, which means that thicker TiO_2 films are superior in terms of light-harvesting ability. However, the gains level off as the thickness increases. In case of TiO_2 NPs, the transmittance depends only on the thickness because of their intrinsic light–transmission properties. The transmittance of TiO_2 NFs, on the other hand, is lower than that of TiO_2 NPs over the entire wavelength range, indicating that the TiO_2 NFs possess greater light scattering abilities. A high degree of scattering can maximize the absorption of the incident light, improve the light harvesting efficiency, and increase J_{sc}. The transmittance of TiO_2 NFs declined up to 8 μm thickness but that of the 10- and 12-μm-thick NFs increased against decreasing the inclination because of inconsistent light scattering.

Owing to randomly aligned TiO_2 NFs (Fig. 3(c)), light harvesting by this nanostructure layer is influenced not only by the thickness but also by various other phenomena such as light scattering, back-scattering, and reflection. Our results indicate that light harvesting in TiO_2 NFs is better than that in TiO_2 NPs because of their long length, large diameter, and light scattering effects. This study, however, is mostly concerned with the double-layered photoanodes that combine the properties of TiO_2 NFs and NPs. The transmittances of the double-layered photoanodes are weaker than that of the single-layers containing only TiO_2 NPs or NFs. In the double-layered photoanodes, an increase in the thickness of the TiO_2 NFs layer improves the scattering effect. However, more dye loading can be achieved using thicker TiO_2 NPs layer in the double-layered photoanode. Hence, it may be possible to obtain significantly improved device performance by controlling the relative thicknesses of the two layers in the photoanode.

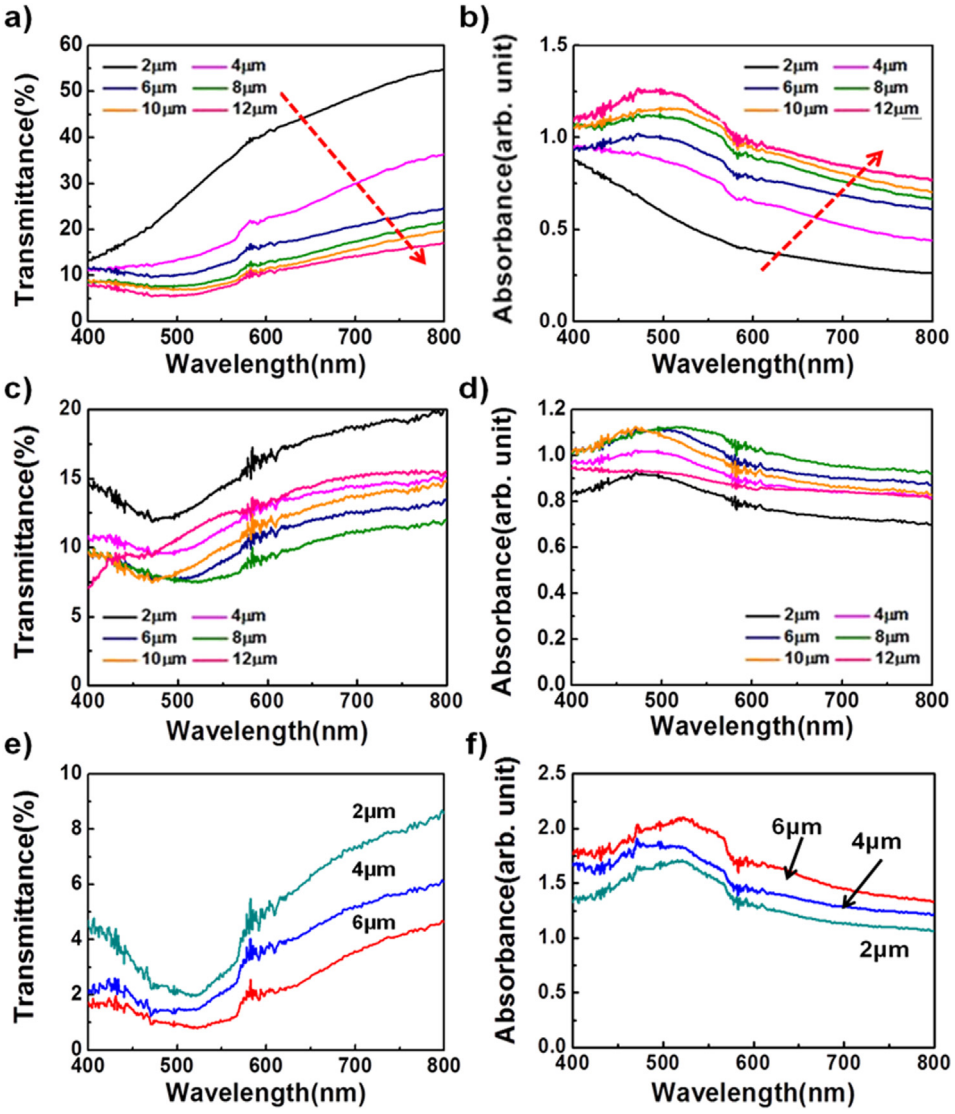

Fig. 4. Transmittance and absorbance spectra of (a, b) TiO_2 NP-based, (c, d) TiO_2 NF-based, and (e, f) double-layered photoanodes as a function of layer thickness. Double-layered photoanodes composed of TiO_2 NP layer and TiO_2 NF layer, and data are displayed according to thickness of NF layer.

As shown in Fig. 4(b), (d) and (f), the absorbance data for TiO_2 NP films, TiO_2 NF films, and TiO_2 double-layer films display a behavior similar to the transmittance data of the samples. Using the optical spectra, we investigated whether TiO_2 NFs act as a scattering layer and whether the thickness of the scattering layer has an effect on light harvesting. Furthermore, to survey the interrelation of light harvesting with electron generation and J_{sc}, the incident photon-to-electron conversion efficiency (IPCE) was measured. Similar to the light harvesting results, the data in Fig. 5(a) indicate that the thinner scattering layer gives higher IPCE values over all wavelengths, except for P25. The IPCE values of the photoanodes with 2- and 4-μm-thick scattering layers showed not only a similar tendency but also improvement over that of P25. This suggests that TiO_2 NFs function as scattering layers if the layer thickness is at least 2 μm. However, the IPCE of photoanode with a 6-μm-thick scattering layer is lower than that of P25. Hence, the thickness of the scattering layer can only improve the scattering effect.

Our results also indicate that the efficiency of a DSSC is not influenced only by its light harvesting capabilities.

$$\mathrm{IPCE}(\lambda) = \frac{1239.8(\mathrm{W\cdot nm/A}) \times J_{SC}(\mathrm{mA/cm^2})}{\lambda(\mathrm{nm}) \times P(\mathrm{mW/cm^2})} \quad (1)$$

According to Eq. (1), the IPCE depends on J_{SC}, and J_{SC} is associated with electron injection, charge collection, and charge recombination within the DSSC. From this point of view, NP/NF double-layered photoanodes are desirable structures for enhancing $J_{sc.}$ The high transmission values of pure P25 photoanodes indicate a large amount of light loss. The introduction of a TiO_2 NF layer encourages light retention inside the DSSC via a scattering effect. As a result, photons might be generated more than those generated without TiO_2 NF layers; IPCE also showed an improvement. Hereby, the IPCE data reflected both light scattering and specific surface area effect.

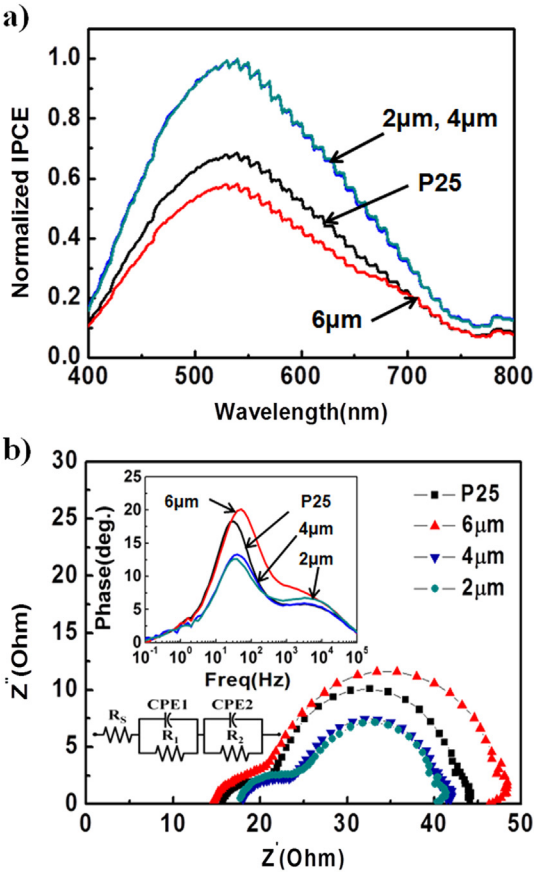

Fig. 5. (a) IPCE and (b) EIS spectra of double-layered photoanodes according to thickness of TiO_2 NF layers. Insets show Bode-phase plot and equivalent circuit model of these DSSCs.

The electrochemical impedance measurements may be confirm the effect of the scattering layer on electron transport and recombination in the double-layered DSSCs. Fig. 5(b) indicates the Nyquist plots related to the interfacial resistance characteristics for the DSSCs under the open-circuit condition. In this study, two semicircles can be recognized and fitted according to an equivalent circuit model (see the inset in Fig. 5(b)), where the finite diffusion element is also represented by the shunt resistance and frequency constant phase element (CPE). The starting point (R_s), the first (R_1), and second (R_2) semicircular curves have been derived from the sheet resistance of FTO, the interfacial resistance of the TiO_2 double-layer/FTO and Pt/electrolyte, and electron transfer at the TiO_2 double-layer/dye/electrolyte interface, respectively. The first semicircle represents the impedance corresponding to charge transfer at the counter electrode (R_1). The second semicircle gives information on the impedance at the TiO_2 double-layer/electrolyte interface (R_2) related to the charge transport/recombination, which is very important for determining the efficiency of these devices. The fitted data are put together in Table 1, which reveal several features. The R_s and R_1 values for the DSSCs are all similar, simply because the counter electrodes and the P25 layer on the FTO/glass were all obtained by the same way. Except for the scattering effect, two factors can be invoked to explain the higher R_2 value of the photoanode with 6-μm-thick scattering layer compared to the P25 layer: a smaller surface area resulting in a larger recombination resistance and less contact points between NFs giving rise to a larger transport resistance. We also found that the R_2 value of the photoanode with 2-μm-thick scattering layer is smaller than that of the photoanode with 4-μm-thick scattering layer. In accordance with the IPCE results, the second semicircle decreased according to the specimen order: 6 μm, P25, 4 μm, and 2 μm. Therefore, the photoanode with the 2-μm-thick scattering layer provides the fastest redox reaction in the electrolyte, good electron transport, and reduced electron recombination. These interpretations are also supported by the Bode-phase plot in the inset.

The electron lifetime (τ_e) in the double-layered photoanodes was evaluated according to $\tau_e = 1/2\pi f_{max}$, where f_{max} is the maximum peak frequency. In comparison with the P25 layer ($\tau_e = 5.37$ ms), the calculated electron lifetimes were 5.05, 4.02, and 3.09 ms for double-layered photoanodes with 2-, 4-, and 6-μm-thick NFs, respectively (Table 1). In this study, the double-layered photoanodes have shorter electron lifetime than that of the P25. This reason is considered to be due to the increase of the thickness of the scattering layer and the decrease of contact or cross points at the interface between NFs and NPs layers. Among double-layered photoanodes, the photoanode with a 2-μm-thick scattering layer showed the longest lifetime, which reflects higher electron transport rates and restrained electron recombination, considering the scattering effect of the NFs.

Table 1
EIS parameters of the DSSCs determined by fitting the experimental data to the equivalent circuit model (see Fig. 5(b)).

Photoanodes	R_S (Ω)	R_1(Ω)	R_2(Ω)	τ_e(ms)
P25(12 μm)	15.71	7.49	19.65	5.37
P25(6 μm)/NFs (6 μm)	14.69	8.87	24.25	3.09
P25(8 μm)/NFs(4 μm)	17.98	7.93	14.47	4.02
P25(10 μm)/NFs(2 μm)	17.66	8.85	13.83	5.05

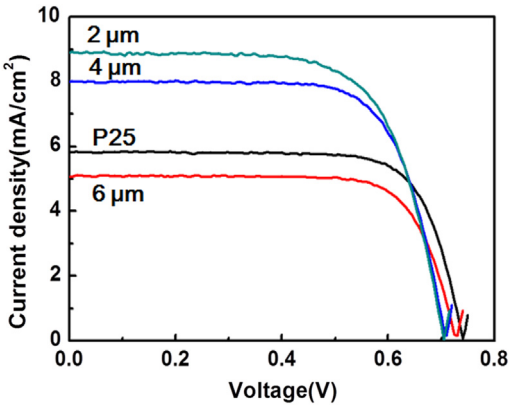

Fig. 6. *J–V* curves of DSSCs with standard TiO_2 NP and double-layered photoanodes. Thicknesses of TiO_2 NF layers were 2, 4, and 6 μm.

Table 2
Performance of DSSCs according to the thickness of scattering layer in double-layered photoanodes.

Photoanodes	J_{sc} (mA/cm^2)	V_{oc} (V)	FF (%)	η(%)
P25(12 μm)	5.84	0.74	73	3.16
P25(6 μm)/NFs (6 μm)	5.11	0.72	72	2.69
P25(8 μm)/NFs(4 μm)	8.05	0.71	69	3.94
P25(10 μm)/NFs(2 μm)	8.92	0.70	67	4.21

For various DSSCs, the variations in the photocurrent density as a function of photovoltage are shown in Fig. 6. Table 2 presents the short-circuit photocurrent per unit area (J_{sc}), open-circuit photovoltage (V_{oc}), fill factor (FF), and power conversion efficiency (η) according to the thickness of the scattering layer in the DSSCs with double-layered photoanodes. Compared with the conventional DSSC with only a P25 photoanode, the efficiency of DSSCs for the 6-μm-thick scattering layer was approximately 17% less. However, the efficiently of the 2- and 4-μm-thick double-layer devices was improved. These differences in the efficiency are mainly caused by the changes in the photocurrent density, a result that could be attributed to the following reasons: first, the specific surface area of the TiO_2 NFs is not higher than that of the P25 used in this experiment. A P25 layer having higher surface area might adsorb more dye and generate more electrons on exposure to the light. Second, TiO_2 NFs have the scattering property that increases the light capture inside the DSSC device, because the dwell time of light in the DSSC is extended. Therefore, the photocurrent density increases.

The highest power conversion efficiency of any DSSC in this study was 4.21%, for the photoanode composed of 10-μm-thick P25 layer and 2-μm-thick TiO_2 NF layer. This efficiency was approximately 33% higher compared to the 3.16% efficiency measured in the specimen with only the P25 layer. Generally, P25 layers with large specific surface area enhance the adsorption of dye and TiO_2 NFs with the light scattering property facilitate the light capture in the DSSCs. However, when the thickness of scattering layer exceeds a certain value, TiO_2 NFs may reflect the light to outside of the DSSCs by back-scattering. Therefore, in the design of a double-layered NP/NF structure, both surface area and scattering effects should be considered when determining the optimum configuration.

4. Conclusion

Because visible light can easily penetrate the transparent P25 layer, the inclusion of an upper scattering layer on the P25 layer is proposed. In this study, a double-layered structure comprising TiO_2 nanofibers on top of the P25 layer was used to increase the absorption of the scattered light in the P25 layer. After introducing the TiO_2 NF layer, the short-circuit current density increased from 5.84 to 8.92 mA/cm^2, while open-circuit voltage remained almost the same. Consequently, the double-layer DSSC showed a higher cell performance than that of the cell with only a P25 layer; the efficiency of the DSSCs was improved from 3.16% to 4.21%. These gains were attributed to the enhanced light scattering capabilities of TiO_2 NFs. This could also be a result of the lower impedance, recombination rate, and longer lifetime in comparison with pure P25 photoanodes.

Acknowledgment

This work was supported by the Financial Supporting Project of Long-term Overseas Dispatch of PNU's Tenure-track Faculty, 2013.

References

[1] B. O'Regan, M. Grätzel, Nature 353 (1991) 737.
[2] S. Ito, T.N. Murakami, P. Comte, P. Liska, C. Grätzel, M.K. Nazeeruddin, M. Grätzel, Thin Solid Films 516 (2008) 4613.
[3] M.K. Nazeeruddin, F.D. Angelis, S. Fantacci, A. Selloni, G. Viscardi, P. Liska, S. Ito, B. Takeru, M. Grätzel, J. Am. Chem. Soc. 127 (2005) 16835.
[4] J. Ferber, J. Luther, Sol. Energy Mater. Sol. Cells 54 (1998) 265.
[5] H.S. Wang, S.Y. Chen, Y.L. Wang, K.H. Wei, J. Nanosci. Nanotechnol. 11 (2011) 3229.
[6] D. Kuang, J. Brillet, P. Chen, M. Takata, S. Uchida, H. Miura, K. Sumioka, S.M. Zakeeruddin, M. Grätzel, ACS Nano 2 (2008) 1113.
[7] K. Ahn, H.U. Lee, Y.M. Jeong, J.P. Kim, S.Y. Jeong, C.R. Cho, J. Nanosci. Nanotechnol. 11 (2011) 1.
[8] S. Ito, P. Chen, P. Comte, M.K. Nazeeruddin, P. Liska, P. Pechy, M. Grätzel, Prog. Photovoltaics 15 (2007) 611.
[9] A. Usami, Chem. Phys. Lett. 277 (1997) 105.
[10] G. Rothenberger, P. Comte, M. Grätzel, Sol. Energy Mater. Sol. Cells 58 (1999) 321.
[11] F. Huang, D. Chen, X.L. Zhang, R.A. Caruso, Y. Cheng, Adv. Funct. Mater. 20 (2010) 1303.
[12] K. Fujihara, A. Kumar, R. Jose, S. Ramakrishna, S. Uchida, Nanotechnology 18 (2007) 365709.
[13] K. Zhu, N.R. Neale, A. Miedaner, A.J. Frank, Nano Lett. 7 (2007) 73.
[14] W. Zhang, R. Zhu, L. Ke, X. Liu, B. Liu, S. Ramakrishna, Small 6 (2010) 2176.
[15] P. Zhu, A.S. Nair, S. Yang, S. Peng, S. Ramakrishna, J. Mater. Chem. 21 (2011) 12210.
[16] L. Yang, W.W. Leung, Adv. Mater. 23 (2011) 4559.
[17] S.H. Hwang, C. Kim, H. Song, S. Son, J. Jang, ACS Appl. Mater. Interfaces 4 (2012) 5287.